White Rose
university consortium
Universities of Leeds, Sheffield & York

eprints@whiterose.ac.uk
https://eprints.whiterose.ac.uk/

Active site isolation in bismuth-poisoned Pd/SiO$_2$ catalysts for selective hydrogenation of furfural

Nikolay Cherkasov[a,b,]*, Antonio José Expósito[a], Moom Sinn Aw[c], Javier Fernández-García[d], Steve Huband[e], Jeremy Sloan[e], Larysa Paniwnyk[c], Evgeny V Rebrov[a,b,f,]*

[a] School of Engineering, University of Warwick, Coventry CV4 7AL, UK

[b] Stoli Catalysts Ltd, Coventry, CV3 4DS, UK

[c] School of Life Sciences, Department of Health and Life Sciences, Coventry University, Alison Gingell Building, Priory Street, Coventry CV1 5FB, UK

[d] School of Chemical and Process Engineering, University of Leeds, LS2 9JT, UK

[e] Department of Physics, University of Warwick, Coventry CV4 7AL, UK

[f] Department of Biotechnology and Chemistry, Tver State Technical University, 170026, Nab. A. Nikitina 22, Russia, E-mails: n. cherkasov@warwick.ac.uk, e.rebrov@warwick.ac.uk

Abstract

Active site isolation in furfural (FA) hydrogenation was studied by poisoning a Pd catalyst with bismuth. A solution of FA in water was hydrogenated over a 5 wt% Pd/SiO$_2$ catalyst in a batch reactor at various reaction temperatures and pressures. Furfuryl alcohol (FAL) was an intermediate product which was further hydrogenated into tetrahydrofurfuryl alcohol (TFAL) or cyclopentanone (CPA) and cyclopentanol (CPOL). While application of hydrogen pressure above 30 bar had little effect on the hydrogenation kinetics, a reaction temperature affected product distribution and the main product changed from TFAL (at 50 °C) to FAL (100 and 150 °C). Poisoning the catalyst with Bi decreased the number of available active sites but had little effect on the turn-over frequencies, most likely because of the absence of electronic effects of Bi on Pd nanoparticles. The main reaction product over the Bi-poisoned catalyst was FAL with no FA oligomerisation products. At a reaction temperature of 150 °C, CPA was formed with a 57 % yield. Considering that Bi preferentially poisons step sites of Pd, the comparison of the product distribution between the Pd and Pd-Bi catalyst as well as the literature data for the alloy Pd-Cu catalysts indicates that the active site isolation observed in the Pd-Bi catalysts is responsible for the increasing FAL and CPA selectivities and elimination of oligomer by-products.

Keywords: hydrogenation; active site; palladium; bismuth; poison

1. Introduction

Renewable fuels and chemicals attract considerable attention due to the depletion of traditional fossil feedstocks [1]. Biomass, however, is highly oxygenated and de-deoxygenation is often have to be performed in order to transform it into more useful or stable chemicals [2,3]. Therefore, biomass utilisation is closely connected to the development of bio-refineries that are able to transform biomass into valuable products [4].

Furfural (FA), a platform chemical for biorefineries [5], can be obtained by the hydrolysis and dehydration of hemicelluloses in agricultural waste [6,7]. Although utilisation of furfural as a biofuel is difficult, many valuable products can be obtained by its hydrogenation [5,8], The FA hydrogenation products include furfuryl alcohol (FAL)[9,10], tetrahydrofurfuryl alcohol (TFAL) [11,12], cyclopentanone (CPA) [8,13], cyclopentanol (CPOL) [14,15], 2-methyltetrahydrofuran [16,17], 2-methylfuran [3,18], furan [19], and other aliphatic molecules formed by the furan ring opening [20]. The number of possible products and complexity of chemistry results in low selectivity to a particular compound [3,21]. A number of catalysts were studied to

increase the product selectivity such as Pt [13,22], Ru [3,4], Pd [23,24], Cu [25,26] and Ni [8,27]. Pd-based catalysts showed one of the highest reaction rates and were studied in both vapour [2,28] and liquid phase hydrogenation [13,17,29–31]. Previous works have demonstrated that furfural forms different attachments on the Pd surface. The selective hydrogenation can vary from the flat-lye conformation generated in terrace sites to the upright conformation in terrace, edges and steps sites.[32].

Poisoning of Pd catalysts with a second metal provides an opportunity to alter the product selectivity and study the hydrogenation reaction pathway [7,28,31,33]. For example, alloying Pd with Ir increases (compared to either Pd or Ir alone) the reaction rate and TFAL selectivity [31]. The change in selectivity over the Pd-Ir alloy catalysts is caused by the adsorption via both the furan and aldehyde groups, while the monometallic Pd and Ir catalysts adsorb furfural predominantly only via either the furan, or the aldehyde groups. Plating Pd with Cu increases the selectivity to CPA in the aqueous-phase furfural hydrogenation [7]. The second metal can also play an active role in stabilisation of the Pd nanoparticle dimensions. A Pd-Sn/SiO_2 catalyst after calcination at the optimum temperature of 450 $^{\circ}$C shows an increased furfural hydrogenation activity, which is attributed to the stabilisation of the 2.5 nm particles [34].

There is little data on the effect of Bi poisoning of Pd catalysts on FA hydrogenation in the literature. Bi, however, is particularly interesting because the nature of the poisoning is well known. Bi atoms predominantly block the step sites of the Pd nanoparticle leaving the flat terraces intact as confirmed by both DFT calculations and infrared spectroscopy studies [35–37]. In our earlier reports [38,39], we demonstrated that Bi-poisoned Pd catalysts show a significant decrease in hydrogenation rates for an internal compared to a terminal alkene. Bi poisoning improves alkene selectivity in terminal alkynol semi-hydrogenation with little electronic effects, thus allowing to decouple spatial and electronic effects of the catalyst on the product selectivity. In this paper we study the effect of Bi poisoning on Pd catalysts to gain a better understanding of spatial effects on FA hydrogenation selectivity.

2. Experimental

2.1. Catalyst preparation

A 5 wt% Pd/SiO_2 catalyst was prepared by wet impregnation. A solution of palladium (II) acetylacetonate (98%, Sigma Aldrich) in toluene (99%, VWR chemicals) filled the pores of the fumed silica (Alfa Aesar, BET specific surface area of 200 $m^2\,g^{-1}$). The impregnated silica was dried in a rotatory evaporator, calcined at 400 $^{\circ}$C for 2 hours in a tube furnace in the flow of air 100 mL min^{-1} and reduced in H_2 flow of 20 mL min^{-1} at 150 $^{\circ}$C for 1 hour. (All gas flow rates are presented at the normal temperature and pressure).

The Bi-poisoned Pd catalyst was prepared by adopting the methodology reported in references [36,38]. Briefly, the reduced 5 wt% Pd/SiO_2 catalyst (700 mg) was dispersed in 20 mL of an aqueous 2 vol% acetic acid solution. A freshly-prepared 20 mM aqueous Bi(NO_3)$_3$ solution in 2 vol% acetic acid was added on stirring at 1500 rpm. The amount of the Bi solution was selected to obtain a Pd/Bi molar ratio of 7 assuming a complete reduction of Bi. The slurry was then stirred for 16 hours at 80 $^{\circ}$C in a static H_2 atmosphere. On cooling, H_2 was replaced with N_2. Finally, the solvent was evaporated in a rotavapour and the sample was passivated by slowly introducing air through a 24-gauge syringe needle into the vial with the catalyst.

2.2. Catalyst characterisation

Transmission electron microscopy (TEM) study was carried out with a Jeol 2010 microscope. The catalysts were suspended in ethanol under sonication and applied on carbon-coated copper grids. The electron images were taken from 10-15 various regions of the grids and analysed using ImageJ [40]. High Resolution TEM and Scanning Transmission Electron Microscopy (STEM) imaging studies were carried out with Jeol ARM200F double aberration corrected instrument operated at 200 kV and equipped with a Gatan Orius

SC1000 CCD camera. Energy Dispersive X-ray (EDX) mapping studies were performed with probe currents of approximately 200 pA and collected with an Oxford Instruments X-max Silicon Drift Detector with an area of 80 mm^2.

Elemental analysis was performed from the solutions of the catalysts dissolved using an inductively coupled plasma spectrometer Perkin Elmer Optima 5300DV. The catalysts were dissolved in a mixture of HF, HCl, and HNO$_3$ (1:1:3 volume ratio) under microwave irradiation at 200 °C. The samples were diluted and compared against standards in the concentration range of 0.1-10 ppm.

X-ray diffraction (XRD) studies were carried out with an Empyrean X-ray diffractometer equipped with monochromatic Cu K$_\alpha$ source and a linear PIXcel detector. The catalyst samples were studied in the 2θ range of 20-85°, step length of 0.04°, and step time of 30 min. Small-angle X-ray scattering measurements were made using a Xenocs Xeuss 2.0 equipped with a micro-focus Cu K$_\alpha$ source collimated with scatterless slits placing the powder catalysts between two Kapton windows. A Pilatus 300k detector with a pixel size of 0.172 μm x 0.172 μm was used to measure scattering. The system was calibrated using silver behenate (AgC$_{22}$H$_{43}$O$_2$) and fitting of the data was performed in the Irena analysis package [41]. Further details are provided in the Supplementary Material.

Chemisorption study of carbon monoxide was performed in a modified system described in reference [42]. The samples were dried in a flow of He (20 mL min^{-1}), calcined in a flow of 5 vol% O$_2$ in He (20 mL min^{-1}) at 300 °C, reduced in a 1 vol% H$_2$ in He mixture (20 mL min^{-1}) at 350 °C. On cooling to room temperature in He, a flow of 0.1 vol% CO, 0.1 vol% Ar in He (6 mL min^{-1}) was introduced through the catalyst bed. A mass spectrometer was used to monitor the concentrations at the outlet, with Ar appearing quickly (which corresponded to the dead volume of the reactor), followed by CO later corresponding to chemisorption on the sample.

The X-ray photoelectron spectra (XPS) were recorded with a Kratos Axis Ultra DLD spectrometer equipped with a monochromated Al Kα X-ray source and operating at 2·10^{-10} mbar pressure. The powdered samples were applied to the electrically-conductive tape and studied at a pass energy of 20 eV from the area of about 0.3 x 0.7 mm. The binding energy and spectrometer work function were calibrated using a polycrystalline Ag sample.

2.3. Hydrogenation experiments

FA (98%, Sigma Aldrich) was distilled under vacuum prior to experiment to remove oligomerisation products. The catalyst (10-50 mg) was introduced together with 90 mL of water into a 160 mL high-pressure stainless Parr batch reactor. Prior to the experiments, the slurry was degassed by flushing N$_2$, 5 times, and H$_2$, 3 times. The reactor was heated up to the desired temperature under a pressure of 2 bar H$_2$. Then, a solution of 500 mM FA was prepared in 20 vol% isopropanol in water and flushed 10 times with 5 bar H$_2$ to remove the dissolved air.

After the reactor had reached the desired temperature, H$_2$ was introduced till the desired hydrogen pressure, and the reaction started when 10 mL of the 500 mM FA solution was injected into the reactor (where 90 mL of water had been placed previously). Liquid samples (0.5 mL) were taken and analysed with a gas chromatograph (Shimadzu GC-2010) equipped with a 30 m x 0.32 mm Stabilwax capillary column and am FID detector.

Conversion of FA (X_{FA}) and selectivity (S_X) were calculated using equations 2 and 3

$$X_{FA} = 1 - \frac{C_{FA}}{C_{FA,in}}, \qquad (2)$$

$$S_X = \frac{C_x}{C_{FA,in} - C_{FA}}, \qquad (3)$$

where C_X is the concentration of a product X and $C_{FA,in}$ is the initial FA concentration in the reactor.

The absence of external mass transfer limitations was verified in a separate series of experiments where the reaction rates did not change with a stirring speed above 600 rpm, while the reaction was performed at 1000 rpm. The highest Weisz-Prater numbers were calculated to be 0.07 for FA and 0.03 for H_2 – both are below the threshold values of 1 and 0.3, respectively, thereby confirming the absence of internal mass transfer limitations.

3. RESULTS AND DISCUSSION

3.1. Catalyst characterisation

Table 1 shows the elemental composition of the catalysts studied. The Pd content in the Pd/SiO$_2$ catalyst agrees with a nominal Pd loading of 5 wt%. The slight decrease in the Pd loading in the Pd-Bi/SiO$_2$ catalyst was likely caused by the increase in total catalyst mass from introducing Bi. The Bi content in the Pd-Bi/SiO$_2$ catalyst corresponded to the Pd/Bi molar ratio of 7.06, which is in excellent agreement with the nominal ratio of 7. Therefore, both Pd and Bi were fully incorporated into the silica support on wet impregnation.

Complete introduction of Bi is not surprising, considering that the Bi solution was evaporated allowing no routes for Bi removal from the catalyst. Therefore, the Bi-containing compounds might have been precipitated in the original form of separate bismuth nitrate or oxide particles rather than poisoning the Pd catalyst. Chemisorption of CO performed on the catalyst (Table 1) confirmed that the CO capacity for the Pd-Bi/SiO$_2$ catalyst decreased substantially compared to the Pd/SiO$_2$ catalyst. Considering that CO adsorbs strongly on Pd but not on Bi, the decrease in the CO chemisorption capacity indicates blockage of the Pd surface with adsorbed Bi species. The average Pd nanoparticle diameter in the Pd/SiO$_2$ catalyst estimated from the total CO capacity was 6.5 nm [43].

Table 1. Elemental composition and CO chemisorption capacity of the catalysts studied.

	Pd/SiO$_2$	Pd-Bi/SiO$_2$
Pd loading (wt%)	5.12	4.87
Bi loading (wt%)	0	1.36
CO capacity (μmol g^{-1})	*59.6*	*37.1*

Fig. 1 shows the powder XRD patterns for the Pd/SiO$_2$ and Pd-Bi/SiO$_2$ catalysts. The patterns demonstrate a broad peak at *2Θ* =22° corresponding to the silica support with its width attributed to small dimensions of the fumed silica particles. Also, there are peaks corresponding to Pd nanoparticles with an average diameter of about 5 nm based on Scherrer's equation. There are no peaks corresponding to Bi in the patterns indicating that Bi particles are either amorphous, or, likely, undetectably small.
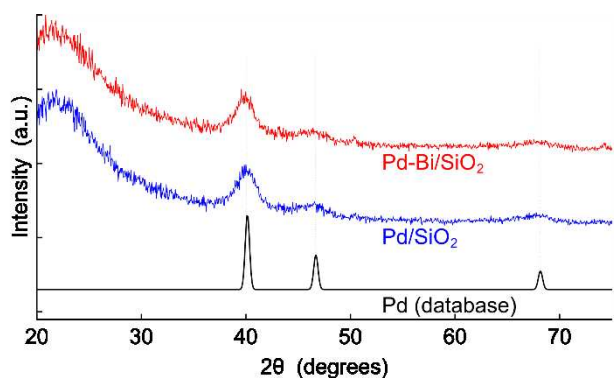
Fig. 1 Powder XRD patterns for the Pd/SiO₂ and Pd-Bi/SiO₂ catalysts.

Fig. 2 shows a representative TEM image of the Pd nanoparticles observed in the Pd/SiO₂ catalyst. The Pd nanoparticles were 7.2±2.0 nm in diameter, which is in good agreement with the XRD and CO chemisorption data. The Pd-Bi/SiO₂ catalyst showed the same nanoparticle morphology and particle size distribution as the Pd/SiO₂ catalyst, which can be explained by the negligible effect of Bi onto the Pd nanoparticle dimensions.
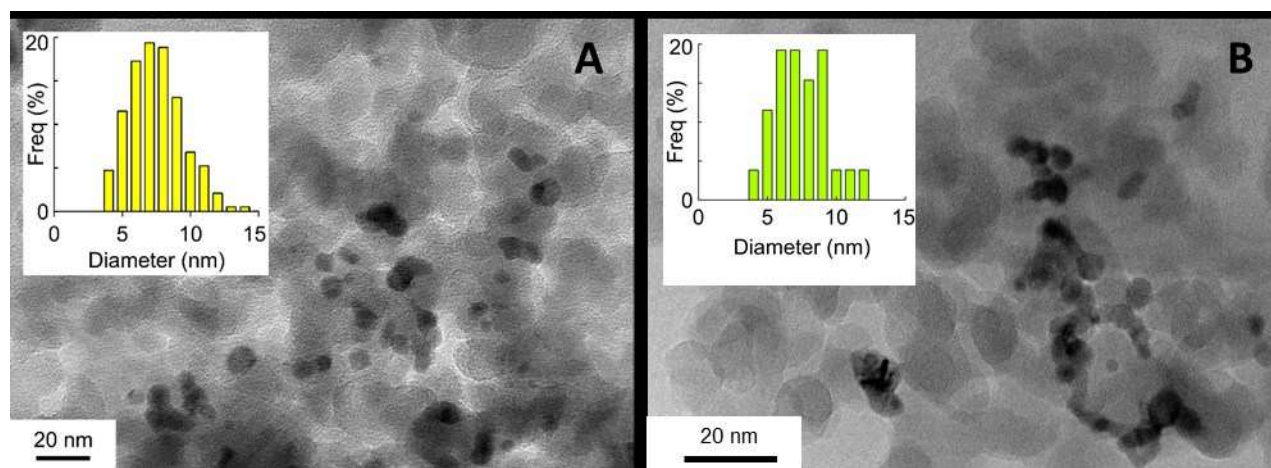

Fig. 2 TEM image of the a) Pd/SiO₂ and b) Pd-Bi/SiO₂ catalyst and the Pd particle size distribution.

The metal nanoparticle dimensions were compared using small-angle X-ray scattering (SAXS) – a method of nanoparticle analysis that provides a more representative analysis compared to microscopy. The scattering data obtained (shown in the Supplementary Material) were fitted using a model of spheres with a lognormal distribution of the radius. It was impossible to distinguish contributions from the Pd and Bi nanoparticles, likely because of the relatively low Bi content. Hence, a combined contribution from both metals was presented. The particle size distributions in Fig. 3 show that the Pd/SiO₂ catalyst had an average nanoparticle diameter of 11.5 nm, while it was 11.0 nm in the Pd-Bi/SiO₂ catalyst. The results are in a fair agreement with the TEM data with the deviation appearing likely from the model selection. Comparison of the SAXS data for the two studied catalysts, however, should be less sensitive to the model selection because of comparable contributions introduced. Therefore, the metal nanoparticle dimensions were very similar for both studied catalysts.
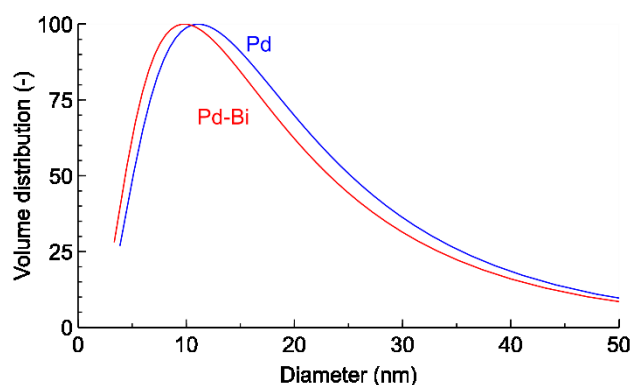
Fig. 3 Metal nanoparticle distribution obtained from the small-angle X-ray scattering studies.

The surface oxidation state of the incorporated Bi and Pd, which refers to the degree of oxidation of the metal in the conditions studied, was studied with ex-situ X-ray photoelectron spectroscopy (Fig. 4). The spectra for the Pd lines studied in the Pd-Bi/SiO$_2$ and Pd/SiO$_2$ catalysts were similar with two peaks corresponding to a single Pd(II) oxidation stage, likely PdO. Formation of the surface oxide was caused by air oxidation during sample transfer. The Bi lines in the Pd-Bi/SiO$_2$ catalyst also contained only one specie – Bi$_2$O$_3$. The formation of PdO in air is known and little effect on the reaction behaviour was expected because reduction to Pd metal in hydrogen takes place even at a room temperature [44]. Reduction of Bi$_2$O$_3$, on the other hand, is significantly more difficult requiring a temperature of about 180 $^{\circ}$C [45]. Therefore, Bi$_2$O$_3$ observed in the Pd-Bi/SiO$_2$ catalyst is likely present during the hydrogenation reactions performed in the work.
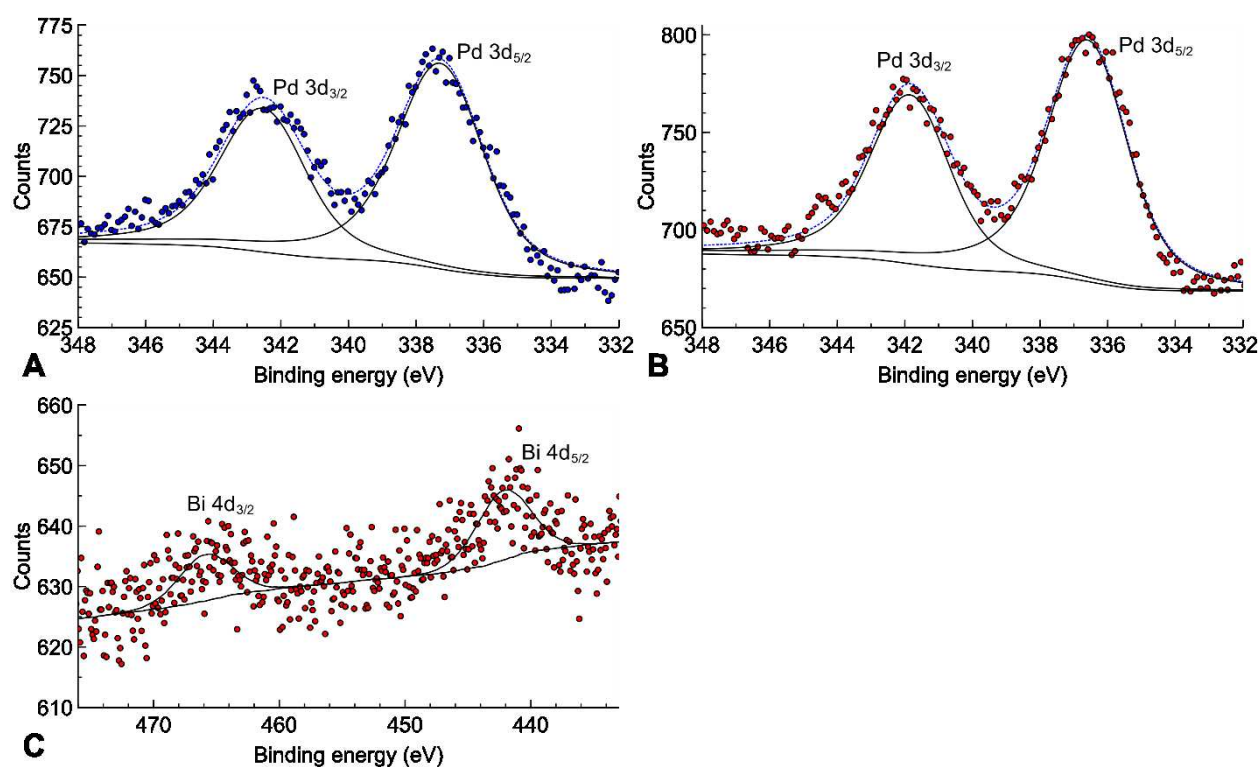

Fig. 4 X-ray photoelectron spectra of the Pd line (A, B) and Bi line (C) for the (A) Pd/SiO$_2$ and (B, C) Pd-Bi/SiO$_2$ catalysts.

Electron diffraction was used to probe the catalyst composition further (Fig. 5). Compared to surface-specific XPS analysis, electron diffraction provides bulk-phase data showing the crystallite phase composition rather

than surface chemical environment. The electron wavelength is also significantly shorter than that of X-rays (Fig. 1), reducing broadening and allowing for more accurate phase identification. The diffraction data presented in Fig. 5 confirm the presence of Pd, PdO, Bi and Bi_2O_3 phases in the Pd-Bi/SiO_2 catalyst.
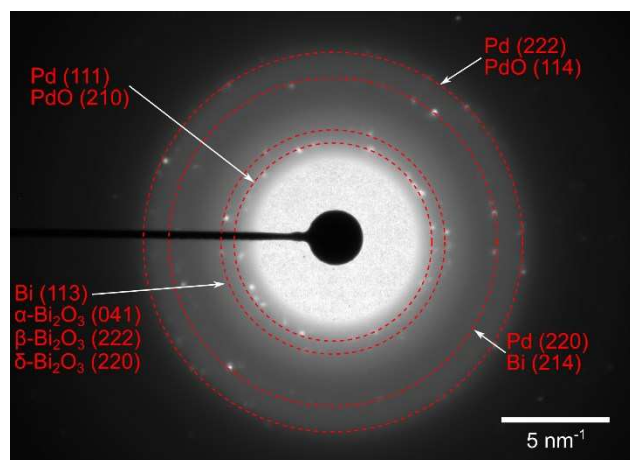

Fig. 5 TEM electron diffraction pattern observed from the metal particles in the Pd-Bi/SiO_2 catalyst.

Further examination of the nanoparticle elemental composition was performed using high-resolution TEM. Fig. 6 shows that the metal nanoparticles preferentially contain Pd. However, a small amount of Bi was also detected in the particles with a Pb/Bi molar ratio of 50 ± 16. The amount of Bi observed over the Pd nanoparticles is significantly lower compared to the bulk content indicating that around 14% of Bi introduced poisoned the Pd nanoparticles.
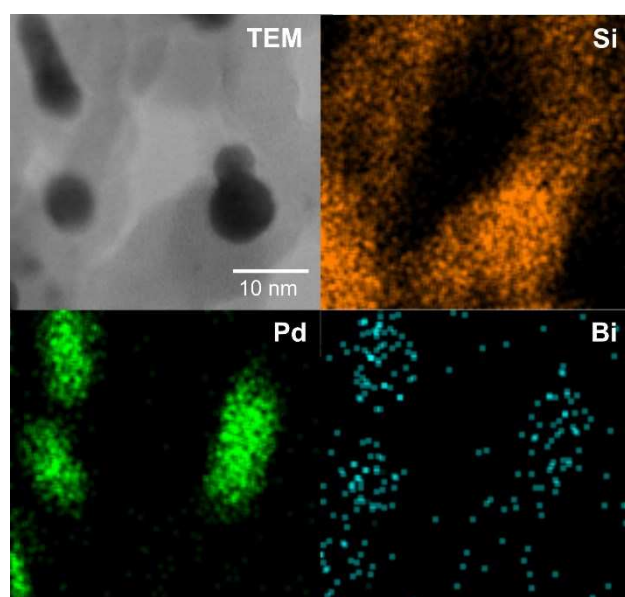

Fig. 6 High-resolution elemental map observed in the Pd-Bi/SiO_2 catalyst.

A combination of the characterisation data indicates that Pd/SiO_2 catalysts contained the Pd nanoparticles of about 7 nm in diameter. The addition of an acidic solution of Bi nitrate under a reducing atmosphere resulted in complete deposition of Bi. However, only a relatively small amount (around 14%) covered the Pd nanoparticles resulting in a negligible change in the metal nanoparticle dimensions. The majority of Bi was precipitated separately as Bi_2O_3 particles – these particles were observed both in XPS spectra and electron diffraction patterns, but are expected to have little effect on the catalyst performance because of their spatial separation from the Pd nanoparticles.

3.2. Hydrogenation over the Pd/SiO₂ catalyst

Fig. 7 shows the concentration profiles and the material balance for FA hydrogenation over the Pd/SiO₂ catalyst under various experimental conditions. The corresponding selectivities to the key intermediates and reaction products are listed in Table 2. Fig. 7 and Table 2 only include the by-products formed in the reaction, although other possible species were analysed.
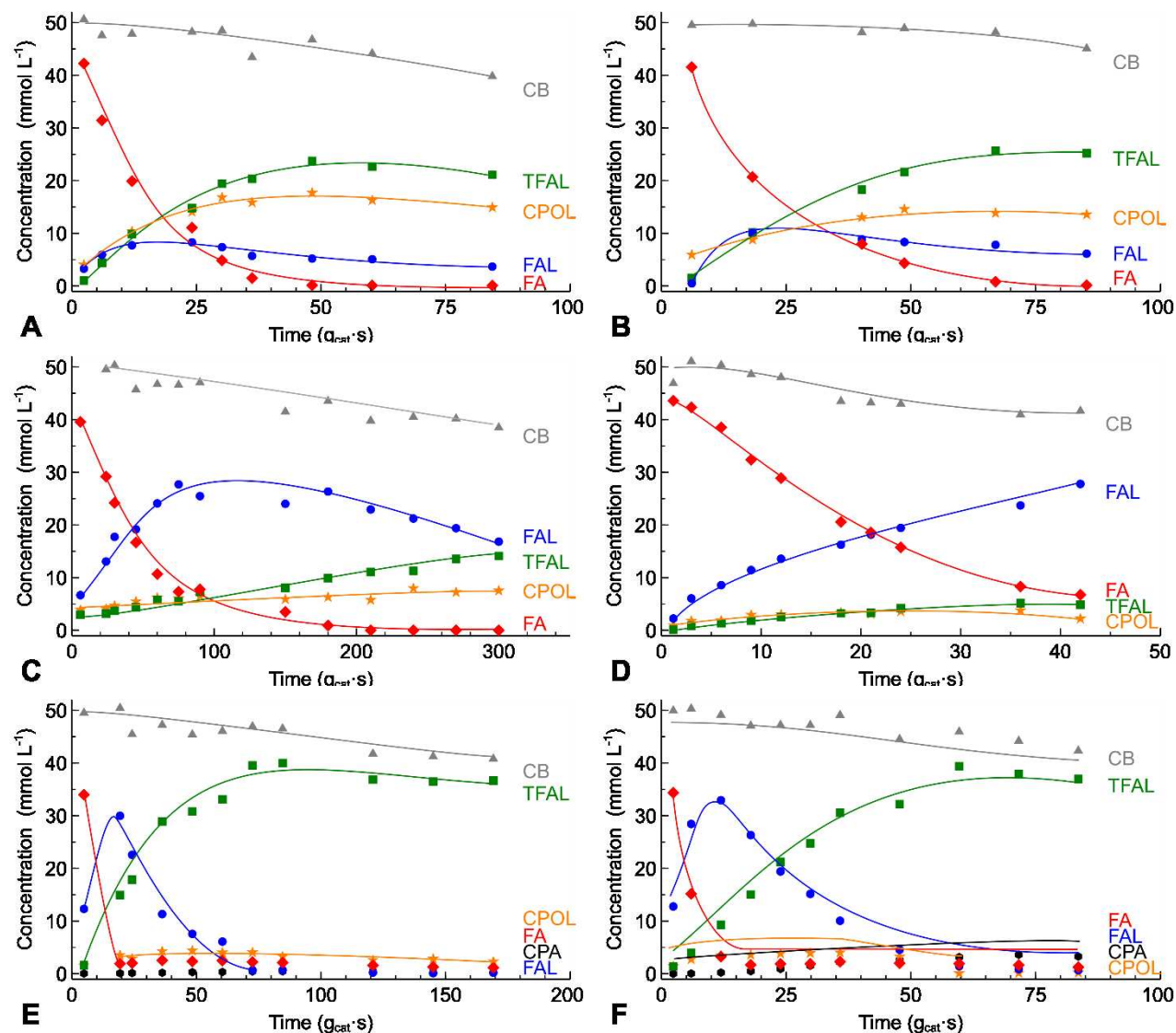

Fig. 7 Concentration profiles for furfural (FA) hydrogenation and the formation of furfuryl alcohol (FAL), tetrahydrofurfuryl alcohol (TFAL), cyclopentanol (CPOL) and cyclopentanone (CPA) as well as the carbon balance (CB). Hydrogenation of a 100 mM FA solution over the Pd/SiO₂ catalyst at (A) 50 °C and 30 bar; (B) 50 °C and 50 bar; (C) 100 °C and 10 bar; (D) 100 °C and 50 bar; (E) 150 °C and 30 bar; (F) 150 °C and 50 bar.

At a reaction temperature of 50 °C, the main reaction products were TFAL and CPOL with minor amounts of FAL. The FAL concentration went through a maximum at the initial reaction stages indicating that FAL was an intermediate reaction product. The comparison of the experiments performed at 30 and 50 bar (Fig. 7A, B) shows that the increasing pressure had a minor effect on the reaction rates and product distribution. The concentrations of TFAL and CPOL increased monotonously with time likely because these compounds were terminal hydrogenation products obtained via parallel reaction routes.

At a reaction temperature of 100 °C, FAL was the major product with a yield above 50%. The reaction rate of FA hydrogenation increased significantly at 50 bar as compared to 10 bar. At a reaction temperature of 150 °C, TFAL was the main product. The TFAL concentration at the later reaction stages was constant indicating that TFAL could not be transformed into CPOL or CPA. For all the temperatures studied, the carbon balance decreased to 85-90%, indicating a formation of undetected products, which are likely oligomers.

The hydrogenation reaction rates are known to be the first order reactions to hydrogen as observed in FA hydrogenation over the Pt, Ru, and Pd catalysts.[34,46–50] The linear relation between pressure and the reaction rate, however, is valid only up to a certain pressure after which the reaction rates become independent on the hydrogen pressure because surface coverage with hydrogen reaches a maximum [51]. Indeed, the reaction pressure had a noticeable effect on the FA hydrogenation reaction rate only at 10 bar (Table 2).

The results observed agree with the literature. The reaction rates increased with the temperature, which is common for Pd, Pt, Ni and Ru catalysts [3,31,34,50,52]. TFAL selectivity decreased with temperature. The DFT calculations for furan hydrogenation and ring opening over the Pd(111) surface suggest that hydrofuran is a reactive intermediate for both pathways [53]. The study suggest that furan ring opening is thermodynamically favoured, while ring hydrogenation is kinetically driven, and hence TFAL formed as a major product at a low temperature.

Similarly, the selectivity to CPA and CPOL is known to increase with temperature. Pt-based catalysts show a rather high CPA selectivity in FA hydrogenation above a reaction temperature of 140 °C [13], while Ni shows the selectivity to CPOL of 50% at 160 °C [27]. Some reports, however, demonstrated that CPA and CPOL selectivity decreases over the Pd catalyst with temperature [31,50].

Table 2 Effect of the experimental conditions on the reaction rates and product selectivity in furfural hydrogenation.

Entry	T (°C)	H$_2$ pressure (bar)	Initial reaction rate[a] (g g$_{cat}^{-1}$ s^{-1})	TOF (s^{-1})	Selectivity at 90% conversion (%)[b]				
					FAL	TFAL	CPOL	CPA	Others
A	50	30	1.64	287	16.3	43.1	37.3	0	3.3
B	50	50	1.57	274	18.3	47.4	32.0	0	2.4
C	100	10	0.99	173	51.7	17.3	12.7	0	18.3
D	100	50	1.69	295	64.3	11.3	5.1	0	19.3
E	150	30	2.46	430	62.3	31.0	7.3	0.2	0
F	150	50	2.69	470	70.5	19.8	7.3	0.5	-

[a]within the first 20 g$_{cat}$·s of reaction. [b] FAL: furfuryl alcohol; TFAL: tetrahydrofurfuryl alcohol; CPOL: cyclopentanol; CPA: cyclopentanone.

Hydrogen pressure had a stronger effect on the product selectivity (Table 2). The TFAL selectivity slightly increased with pressure at the temperature of 50 °C. The selectivity to CPA and CPOL were the most affected by the hydrogen pressure at a reaction temperature of 150 °C. The experiment agrees with the literature data of increasing TFAL selectivity with pressure over the Pd-based catalysts [13,29,31].

From the concentration profiles obtained, the furfural hydrogenation pathway can be summarised in Fig. 8. The pathway agrees with that observed over Ni catalysts [54]. The catalytic behaviour between Pd and Ni with furfural is similar, although Ni forms stronger bonds with the furan ring that can yield the opening of the ring [2]. Side reactions such as furfural decarbonylation to form furan and CO were previously reported by several authors [2,21,22]. The previous reports suggest that the ring opening presumably occurs via the

hydrodeoxygenation of FAL alcohol over the Pd surface [21,55]. Ring opening, however, was not observed during the current study. Below 150 °C, our results agree with the study of Bhogeswararao and Srinivas who found that hydrogenation of furfural is favoured over Pd at temperatures below 180 °C [56].
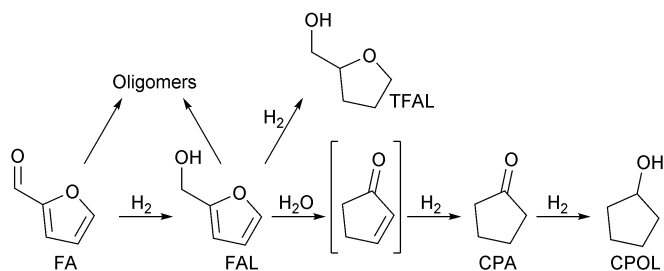

Fig. 8 Proposed pathway for furfural hydrogenation in aqueous phase over the 5% Pd/SiO$_2$ catalyst.

The first step (Fig. 8) is FA hydrogenation to FAL. FAL can undergo further hydrogenation to TFAL. Hronec and Fulajtarová found that FA hydrogenation leads to the production of CPA in water while FAL or TFAL are generated in other solvents [13]. In an aqueous solution, the furan ring is attacked forming 2-cyclopentenone [7]. 2-cyclopentenone was not detected in the current work, likely because it was rapidly hydrogenated into CPA. A further hydrogenation of CPA to CPOL is also possible [13]. Furthermore, FAL and FA can polymerize forming non-volatile products undetectable by gas chromatography [7], which is the likely reason for the decreasing carbon balance in the experiments (Fig. 7).

3.3. Poisoning with bismuth

Isolation of the active sites and electronic effects can be introduced into the catalyst by adding a second metal such as Pb, Au, Cu [57–62]. We have decided to investigate the effect of the addition of Bi because it preferentially adsorbs on the step and edge sites of Pd [36,37]. Therefore, the Bi-poisoned Pd catalyst has predominantly terrace active sites available for hydrogenation. The concentration profiles of FA hydrogenation over the Bi-poisoned catalysts are presented in Fig. 9 and the corresponding selectivity to the main reaction products are summarized in Table 3.

The Pd-Bi/SiO$_2$ catalyst, compared to Pd/SiO$_2$, showed considerably lower initial FA hydrogenation reaction rates under all the temperatures studied (Table 3). It was expected considering that Bi blocked a significant fraction of the Pd active sites. The comparison of the turn-over frequencies (TOF, which normalise the reaction rate by the number of active sites), however, provides comparable values. The TOF for the Pd/SiO$_2$ catalyst was only 10-25% higher than that of the Pd-Bi/SiO$_2$ catalyst. This indicates absence of significant electronic effects, in agreement with the data for alkynol semi-hydrogenation [38]. The difference observed might be caused by spatial limitations as blocking one Pd site may decrease the availability of nearby Pd sites for adsorption of bulky molecules.
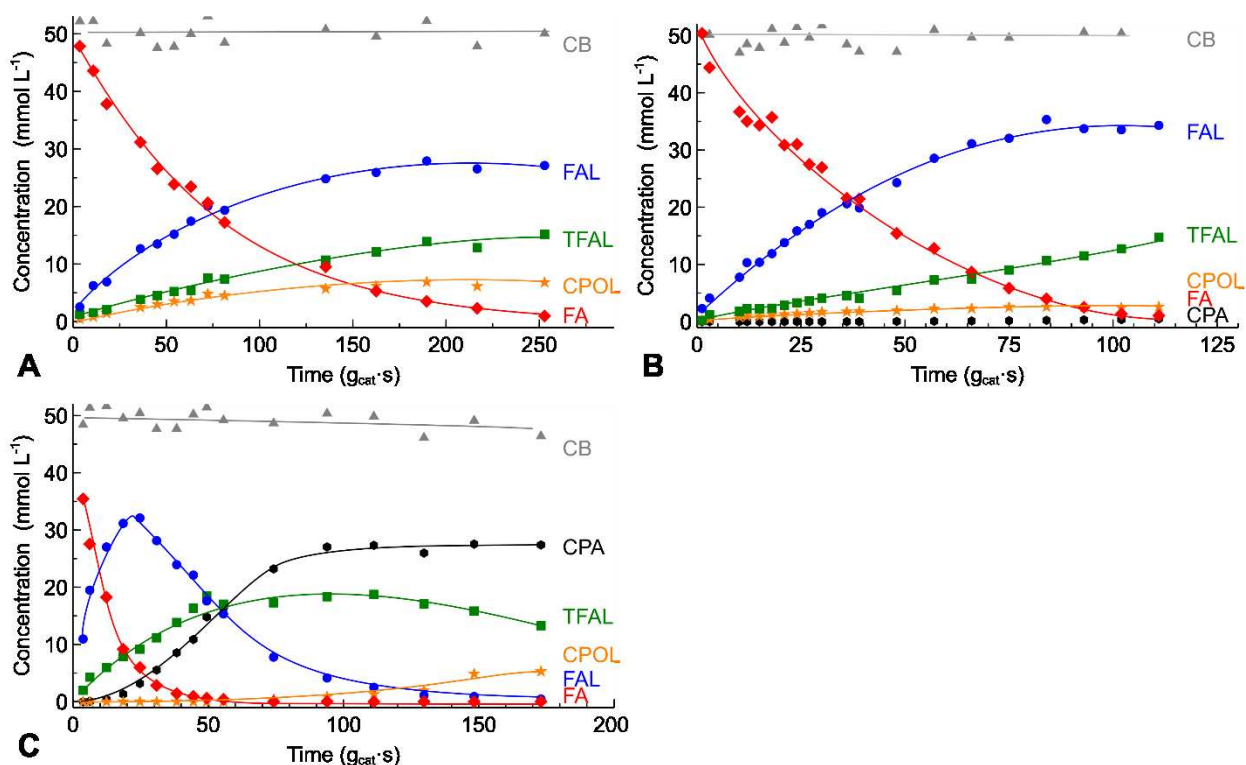
Fig. 9 Concentration profiles for furfural (FA) hydrogenation and the formation of furfuryl alcohol (FAL), tetrahydrofurfuryl alcohol (TFAL), cyclopentanol (CPOL) and cyclopentanone (CPA) as well as the carbon balance (CB). Hydrogenation of a 100 mM FA solution over the Pd-Bi/SiO₂ catalyst at (A) 50 °C and 50 bar; (B) 100 °C and 50 bar; (C) 150 °C and 50 bar.

At a reaction temperature of 50 °C (Fig. 9), the main reaction products were FAL and TFAL with a small amount of CPOL. The Pd-Bi/SiO₂ catalyst, compared to Pd/SiO₂, showed a considerably higher selectivity to FAL and a lower selectivity to CPOL. Moreover, the carbon balance for the reaction conducted with the poisoned catalyst was stable over time indicating no significant product decomposition or polymerisation.

At a reaction temperature of 100 °C, the main reaction product was FAL. Over the Bi-poisoned catalyst, the FAL selectivity did not change significantly compared to the unpoisoned catalyst, but unidentified products were completely eliminated producing TFAL instead.

At a reaction temperature of 150 °C, FAL and TFAL were the main reaction products in the beginning of the reaction over the Pd-Bi/SiO₂ catalyst – the behaviour similar to the Pd/SiO₂ catalyst. Later during the reaction, however, CPA was the main product with a yield factor of 8.3 higher compared to the unpoisoned catalyst. The carbon balance over the Pd-Bi/SiO₂ catalyst was also considerably higher compared to Pd/SiO₂ decreasing somewhat only after 100 g$_{cat}$·s. The likely reason for the reduction in the carbon balance is TFAL evaporation during sampling. The maximum TFAL yield decreased from 78% to 37% on poisoning the Pd/SiO₂ catalyst.

Formation of CPA in FA hydrogenation is mainly favoured under a high reaction temperature of 150 °C with a maximum yield observed of almost 57%. Over the Pd/SiO₂ catalyst, the dominant reaction is hydrogenation of FAL to TFAL, while the Pd-Bi/SiO₂ catalyst showed a formation of both TFAL and CPA in comparable quantities. Therefore, Bi-poisoning of the Pd catalyst affects the reaction of FAL with water to a lesser extent compared to hydrogenation of FAL to TFAL. Additionally, the Bi-poisoned catalyst showed little CPOL formation indicating that the CPA to CPOL hydrogenation was limited.

Table 3 Effect of the reaction conditions in the hydrogenation of furfural over the Bi-Pd/SiO$_2$ catalyst.

Entry	T (ºC)	H$_2$ pressure (bar)	Initial reaction rate[a] (g g$_{cat}^{-1}$ s^{-1})	TOF (s^{-1})	Selectivity at 90 % conversion (%)				
					FAL	TFAL	CPOL	CPA	Others
A	50	50	0.79	222	60.1	29.9	14.9	0	0
B	100	50	0.96	270	76.8	23.2	5.7	0.5	0
C	150	50	2.11	592	72.9	20.8	0	7.2	0

[a]within the first 20 g$_{cat}$·s of reaction. [b]FAL: furfuryl alcohol; TFAL: tetrahydrofurfuryl alcohol; CPOL: cyclopentanol; CPA: cyclopentanone.

Table 4 shows the CPA selectivity obtained from FA hydrogenation in the current work compared to the literature. All the studies were carried out at a reaction temperature above 130 ^{o}C with the CPA yield above 50%. The highest yield of 96% was obtained over the Cu-Ni [63] and 92% over the Pd-Cu catalysts [7].

The comparison of the results obtained over the Pd-Cu and Pd-Bi catalysts is particularly interesting because the effect of Cu onto Pd nanoparticles is well studied. Poisoning Pd with Cu, according to literature, increases the FAL selectivity at low temperature and the CPA selectivity at a higher temperature [7,25,33,64]. Depending on the catalyst preparation method, however, the origins of the effect may be different. Lesiak et al.[64] observed the formation of Pd-Cu alloys, which affected both the FAL selectivity and FA hydrogenation rate via electronic effects. Sitthisa et al.[25] also formed an alloy which decreased the gas-phase reaction rate by reducing the FA decarbonylation rate, but increased the hydrogenation rate. Hronek and co-workers [7,33] observed an increasing FAL selectivity in liquid-phase FA hydrogenation attributed to the proximity of Cu(I) and Pd species. Therefore, the Pd-Bi and Pd-Cu catalysts showed very similar effects on FA hydrogenation despite a different nature of Pd modification.

Table 4 A summary of the literature data on the yield (Y) of cyclopentanone (CPA) in the furfural hydrogenation.

Ref.	Catalyst	T (ºC)	P (bar)	t (hours)	Y (%)
Hronec et al.[13]	Pt / C	160	80	0.5	76.5
Hronec et al.[13]	Pd / C	160	30	1	67.1
Hronec et al.[13]	Ru / C	175	80	1	57.3
Hronec et al.[7]	Pd-Cu / C	160	30	1	92.1
Yang et al.[65]	Ni-Cu / SBA-15	160	40	4	60.0
Zhou et al.[15]	Cu-Mg-Al hydrotalcite	160	40	10	7.4
Liu et al.[8]	Ni / HY zeolite	150	40	9	86.5
Xu et al.[27]	Raney Ni	180	10	4	39.0
Wang et al.[63]	Cu-Ni / C	130	50	5	96.9
Wang et al.[10]	Cu-Co / C	140	30	-	23.4
Ma et al.[14]	Co / ZrO$_2$-La$_2$O$_3$	160	20	-	56.0
Zhou et al.[66]	Cu / Carb. nanotubes	140	40	8	65.5
This work	Pd / SiO$_2$	150	50	1.7	7.4
This work	Pd-Bi / SiO$_2$	150	50	2.3	54.6

Similarity in the behaviour despite a different Pd poisoning mechanism may be reconciled considering the active site isolation. In fact, the Pd-Cu alloy catalyst (with the Cu atoms poisoning the Pd sites uniformly) [37] and the Pd-Bi catalyst (with Bi blocking mainly the edge sites) [36,37] both isolate the Pd sites. The

decreasing FA oligomerisation on Pd poisoning becomes obvious considering that the probability of having two nearby adsorbed FA molecules decreases along with the number of nearby active sites. Therefore, the observed increase in the FAL selectivity over the Bi-poisoned catalyst is explained by the decreasing FA oligomerisation caused by isolation of the Pd active sites.

The increasing CPA selectivity at 150 $^{\circ}$C can also be explained in the same terms by Pd active site isolation over both the Pd-Cu and Pd-Bi catalysts. At the initial reaction stage, FA hydrogenation results in the formation of the FAL molecules (Fig. 8). At a later stage, FAL may form either (i) TFAL via the furan ring hydrogenation or (ii) CPA via the reaction with water followed by hydrogenation of the C=C bond in the cyclopentene ring (Fig. 10). The furan ring hydrogenation requires adsorption over a significantly larger area with the addition of several H_2 molecules in short succession [67]. The C=C bond hydrogenation, on the contrary, requires only one H_2 molecule and a smaller adsorption space due to flexibility of the cyclopentene ring.

Therefore, once the reaction temperature becomes sufficiently high to sustain FAL hydration, the subsequent hydrogenation to CPA becomes dominant. In fact, Bi poisoning almost halved the TFAL formation rate – it was 85 μmol·g_{cat}^{-1}·s^{-1} over the Pd catalyst and only 36 μmol·g_{cat}^{-1}·s^{-1} over the Pd-Bi/SiO$_2$ catalyst. The poisoned Pd catalysts with isolated active sites show a decreased FAL hydrogenation rate allowing for a higher CPA formation. Hydrogenation of one bond in the cyclopentene ring, on the other hand, requires only one hydrogenation step that can be performed over an isolated Pd site.
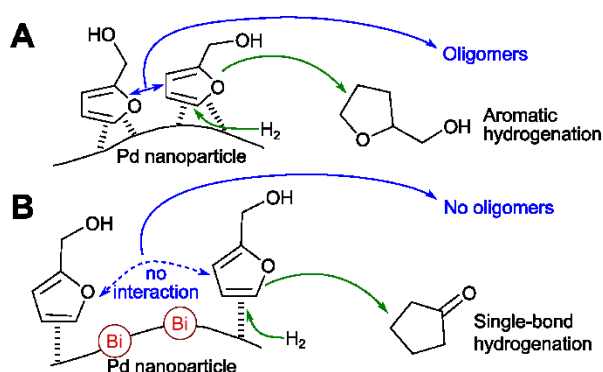

Fig. 10 Scheme of the effect of Bi poisoning on furfural hydrogenation pathways.

Conclusions

Bismuth was deposited onto the Pd catalysts from an aqueous solution. Characterisation of the catalysts showed that the majority of Bi precipitated as Bi_2O_3. But about 14% Bi deposited onto the Pd nanoparticles blocking a fraction of the available Pd surface area. The Bi-poisoned Pd catalysts showed a different behaviour in furfural hydrogenation. Compared to the initial Pd catalyst, the Bi-poisoned catalyst supressed oligomerisation of furfural and increased the formation of cyclopentanol at a higher reaction temperature.

The change in the product selectivity on Bi poisoning can be explained in terms of active site isolation. The addition of Bi decreases the size of the Pd active site ensembles reducing adsorption of furfural via the aromatic ring. The lower site density decreases the probability of adsorption of furfural molecules nearby and their inter-reaction leading to oligomerisation. Similarly, separation of active sites makes single-site reactions such as cyclopentanone formation preferred over the aromatic ring hydrogenation.

Conflicts of interest

There are no conflicts to declare.

References

[1]   S. Proskurina, J. Heinim, F. Schipfer, E. Vakkilainen, Renew. Energy 111 (2017) 265–274.

[2]   S. Sitthisa, D.E. Resasco, Catal. Letters 141 (2011) 784–791.

[3]   P. Panagiotopoulou, N. Martin, D.G. Vlachos, J. Mol. Catal. A Chem. 392 (2014) 223–228.

[4]   Q. Yuan, D. Zhang, L. van Haandel, F. Ye, T. Xue, E.J.. Hensen, Y. Guan, J. Mol. Catal. A Chem. 406 (2015) 58–64.

[5]   K. Yan, G. Wu, T. La, C. Jarvis, Renew. Sustain. Energy Rev. 38 (2014) 663–676.

[6]   J. Lange, E. Van Der Heide, J. Van Buijtenen, R. Price, ChemSusChem 5 (2012) 150–166.

[7]   M. Hronec, K. Fulajtárová, I. Vávra, T. Soták, E. Dobročka, M. Mičušík, Appl. Catal. B Environ. 181 (2016) 210–219.

[8]   C. Liu, R. Wei, G. Geng, M. Zhou, L. Gao, G. Xiao, Fuel Process. Technol. 134 (2015) 168–174.

[9]   M.S. Kim, F.S.H. Simanjuntak, S. Lim, J. Jae, J. Ha, H. Lee, J. Ind. Eng. Chem. 52 (2017) 59–65.

[10]   Y. Wang, Y. Miao, S. Li, L. Gao, G. Xiao, Mol. Catal. 436 (2017) 128–137.

[11]   L. Liu, H. Lou, M. Chen, Int. J. Hydrogen Energy 41 (2016) 14721–14731.

[12]   X. Chen, W. Sun, N. Xiao, Y. Yan, S. Liu, Chem. Eng. J. 126 (2007) 5–11.

[13]   M. Hronec, K. Fulajtarová, Catal. Commun. 24 (2012) 100–104.

[14]   Y. Ma, H. Wang, G. Xu, X. Liu, Y. Zhang, Y. Fu, Chinese Chem. Lett. 28 (2017) 1153–1158.

[15]   M. Zhou, Z. Zeng, H. Zhu, G. Xiao, R. Xiao, J. Energy Chem. 23 (2014) 91–96.

[16]   W. Xu, H. Wang, X. Liu, J. Ren, Y. Wang, G. Lu, Chem. Commun. 47 (2011) 3924–3926.

[17]   M. Hronec, K. Fulajtárova, M. Mičušik, Appl. Catal. A Gen. 468 (2013) 426–431.

[18]   B. Wang, C. Li, B. He, J. Qi, C. Liang, J. Energy Chem. (2017) 1–9.

[19]   M.F. Fellah, Appl. Surf. Sci. 405 (2017) 395–404.

[20]   H. Liu, Z. Huang, H. Kang, C. Xia, J. Chen, Chinese J. Catal. 37 (2016) 700–710.

[21]   V. Vorotnikov, G. Mpourmpakis, D.G. Vlachos, ACS Catal. 2 (2012) 2496–2504.

[22]   R. V. Maligal-Ganesh, C. Xiao, T.W. Goh, L.L. Wang, J. Gustafson, Y. Pei, Z. Qi, D.D. Johnson, S. Zhang, F. Tao, W. Huang, ACS Catal. 6 (2016) 1754–1763.

[23]   M.D. Quian, J.L. Xue, S.J. Xia, Z.M. Ni, J.H. Jiang, Y.Y. Cao, J. Fuel Chem. Technol. 45 (2017) 34–42.

[24]   S.H. Pang, C.A. Schoenbaum, D.K. Schwartz, J. Will Medlin, ACS Catal. 4 (2014) 3123–3131.

[25]   S. Sitthisa, T. Sooknoi, Y. Ma, P.B. Balbuena, D.E. Resasco, J. Catal. 277 (2011) 1–13.

[26]   S.H. Pang, N.E. Love, J.W. Medlin, J. Phys. Chem. Lett. 5 (2014) 4110–4114.

[27]   Y. Xu, S. Qiu, J. Long, C. Wang, J. Chang, J. Tan, Q. Liu, L. Ma, T. Wang, Q. Zhang, RSC Adv. 5 (2015) 91190–91195.

[28]   N. Pino, S. Sitthisa, Q. Tan, T. Souza, D. López, D.E. Resasco, J. Catal. 350 (2017) 30–40.

[29]   W. Yu, Y. Tang, L. Mo, P. Chen, H. Lou, X. Zheng, Bioresour. Technol. 102 (2011) 8241–8246.

[30]   D. Scholz, C. Aellig, I. Hermans, ChemSusChem 7 (2014) 268–275.

[31]   Y. Nakagawa, K. Takada, M. Tamura, K. Tomishige, ACS Catal. 4 (2014) 2718–26.

[32]   S.H. Pang, C.A. Schoenbaum, D.K. Schwartz, J. Will Medlin, ACS Catal. 4 (2014) 3123–3131.

[33]   K. Fulajtárova, T. Soták, M. Hronec, I. Vávra, E. Dobročka, M. Omastová, Appl. Catal. A Gen. 502 (2015) 78–85.

[34]   A. O'Driscoll, T. Curtin, W.Y. Hernández, P. Van Der Voort, J.J. Leahy, Org. Process Res. Dev. 20 (2016) 1917–1929.

[35]   J. Sá, J. Montero, E. Duncan, J.A. Anderson, Appl. Catal. B Environ. 73 (2007) 98–105.

[36]   J.A. Anderson, J. Mellor, R.P.K. Wells, J. Catal. 261 (2009) 208–216.

[37]   N. López, C. Vargas-Fuentes, Chem. Commun. 48 (2012) 1379–1391.

[38]   N. Cherkasov, A.O. Ibhadon, A.J. McCue, J.A. Anderson, S.K. Johnston, Appl. Catal. A Gen. 497 (2015) 22–30.

[39]   N. Cherkasov, A.O. Ibhadon, E. V Rebrov, Appl. Catal. A Gen. 515 (2016) 108–115.

[40]   C.A. Schneider, W.S. Rasband, K.W. Eliceiri, Nat. Methods 9 (2012) 671–675.

[41]   J. Ilavsky, P.R. Jemian, J. Appl. Crystallogr. 42 (2009) 347–353.

[42]   Y. Bai, N. Cherkasov, S. Huband, D. Walker, R. Walton, E. Rebrov, Catalysts 8 (2018) 1–18.

[43]   A. Borodziński, M. Bonarowska, Langmuir 13 (1997) 5613–5620.

[44]   K. Noack, H. Zbinden, R. Schlögl, Catal. Letters 4 (1990) 145–155.

[45]   H. Miura, Y. Morikawa, T. Shirasaki, J. Catal. 28 (1975) 22–28.

[46]   D. Duca, L.F. Liotta, G. Deganello, J. Catal. 154 (1995) 69–79.

[47]   N. Cherkasov, M. Al-Rawashdeh, A.O. Ibhadon, E. V Rebrov, Catal. Today 273 (2016) 205–212.

[48]   Z. Wu, N. Cherkasov, G. Cravotto, E. Borretto, A.O. Ibhadon, J. Medlock, W. Bonrath, ChemCatChem 7 (2015) 952–959.

[49]   S. Vernuccio, R. Goy, A. Meier, P. Rudolf von Rohr, J. Medlock, Chem. Eng. J. 316 (2017) 121–130.

[50]   R.M. Mironenko, O.B. Belskaya, T.I. Gulyaeva, A.I. Nizovskii, A. V Kalinkin, V.I. Bukhtiyarov, A. V Lavrenov, V.A. Likholobov, Catal. Today 249 (2015) 145–152.

[51]   W. Rachmady, M. Vannice, J. Catal. 192 (2000) 322–334.

[52]   L. Baijun, L. Lianhai, W. Bingchun, C. Tianxi, Katsuyoshi Iwatani, Appl. Catal. A Gen. 171 (1998) 117–122.

[53]   S. Wang, V. Vorotnikov, D.G. Vlachos, Green Chem. 16 (2014) 736–747.

[54] B. Yang, J. Zuo, X. Tang, F. Liu, X. Yu, X. Tang, H. Jiang, L. Gan, Ultrason. Sonochem. 21 (2014) 1310–1317.

[55] B. Chen, F. Li, Z. Huang, G. Yuan, Appl. Catal. A Gen. 500 (2015) 23–29.

[56] S. Bhogeswararao, D. Srinivas, J. Catal. 327 (2015) 65–77.

[57] C. Moreno-Marrodan, F. Liguori, P. Barbaro, Beilstein J. Org. Chem. 13 (2017) 734–754.

[58] M. Armbrüster, M. Behrens, F. Cinquini, K. Föttinger, Y. Grin, A. Haghofer, B. Klötzer, A. Knop-Gericke, H. Lorenz, A. Ota, S. Penner, J. Prinz, C. Rameshan, Z. Révay, D. Rosenthal, G. Rupprechter, P. Sautet, R. Schlögl, L. Shao, L. Szentmiklósi, D. Teschner, D. Torres, R. Wagner, R. Widmer, G. Wowsnick, ChemCatChem 4 (2012) 1048–1063.

[59] A.J. McCue, A. Guerrero-Ruiz, C. Ramirez-Barria, I. Rodríguez-Ramos, J.A. Anderson, J. Catal. 355 (2017) 40–52.

[60] S.K. Johnston, N. Cherkasov, E. Pérez-Barrado, A. Aho, D.Y. Murzin, A.O. Ibhadon, M.G. Francesconi, Appl. Catal. A Gen. 544 (2017) 40–45.

[61] S. Gonzalez, K.M. Neyman, S. Shaikhutdinov, H.-J. Freund, F. Illas, J. Phys. Chem. C 2 (2007) 6852–6856.

[62] F. Zaera, ACS Catal. 7 (2017) 4947–4967.

[63] Y. Wang, S. Sang, W. Zhu, L. Gao, G. Xiao, Chem. Eng. J. 299 (2016) 104–111.

[64] M. Lesiak, M. Binczarski, S. Karski, W. Maniukiewica, J. Rogowski, E. Szubiakiewicz, Berlows, "Journal Mol. Catal. A, Chem. 395 (2014) 337–348.

[65] Y. Yang, Z. Du, Y. Huang, F. Lu, F. Wang, J. Gao, J. Xu, Green Chem. 15 (2013) 1932–1940.

[66] M. Zhou, J. Li, K. Wang, H. Xia, J. Xu, J. Jiang, Fuel 202 (2017) 1–11.

[67] A. Stanislaus, H.C. Barry, Catal. Rev. 36 (1994) 75–123.